Solid Freeform Fabrication 2024: Proceedings of the 35th Annual International Solid Freeform Fabrication Symposium – An Additive Manufacturing Conference
Reviewed Paper

RF Sensitive Sensors, Circuits, and Interconnects Using Additive Materials and Techniques

Christopher Molinari[1], Shawn Kelliher [1], Jotham Kasule [1], Lucas Unger[1], Michelle Connolly[1], Basil Vanderbie [1], Samuel Fedorka [1], Gary Walsh[2], Corey Shemelya[1*]
[1]Department of Electrical Engineering, University of Massachusetts Lowell, Lowell, MA 01854
[2]U.S. Army DEVCOM Soldier Center, Natick, MA 01760
*corey_shemelya@uml.edu

ABSTRACT

Additive manufacturing has the potential to revolutionize how RF electronics are designed by enabling the fabrication of electromagnetic structures on nontraditional materials, substrates, and in novel geometries. These new design opportunities allow significant flexibility when implementing new electronics but are also constrained by numerous challenges including surface roughness and reliability. Additionally, the interfaces between discrete IC packages and conductive inks typically suffer from low long-term reliability due to electrical shorts and poor adhesion. Some methods to overcome these challenges include the use of anisotropic conductive epoxies, printed press-fit PCB interconnects, RF-transparent protective coatings, and additively manufactured interposer designs. Each of these solutions overcomes specific challenges within the field of additive manufacturing for electronics; and when the solutions are brought together, the resulting devices will be able to demonstrate unique functionality in novel form factors.

Keywords: Additively manufactured electronics, aerosol jet, stereolithography, radio frequency, anisotropic conductive films

Introduction

Since its inception, additive manufacturing (AM) has been applied to an ever-increasing number of use cases that utilize numerous techniques, materials, and methods. One of these applications is AM for radio frequency (RF) electronics. Both passive RF devices, such as frequency-selective circuits [1], transmission lines [2], and antennas [3] [4] [5] [6], along with active components, including transistors [7] and amplifiers [8] have been successfully demonstrated using AM techniques. Furthermore, the advantages of AM have enabled device implementation in form-factors that are impossible using conventional methods, i.e. conformal [9] [10] [11], nested [12], and gradient index structures [13] integrated directly into existing mechanical systems. Although AM for RF applications has been successful in a variety of cases, there are numerous challenges when moving towards techniques that can utilize AM's advantage of "printing anywhere." For example, there has been significant effort creating RF structures on novel materials including fabrics, films, and other non-traditional substrates [14]. However, these substrates often possess unknown electromagnetic properties [15], highly variable feature resolution [16], poor ink adhesion [17], and variable surface roughness [18]. Additionally, conductive nanoparticle inks are often used in these applications and must have both the appropriate rheological properties for adhesion and sufficiently low sintering temperatures to ensure printability [19].

With respect to printable inks, effects such as “bleeding,” high surface roughness, and poor adhesion have been observed when using non-fully dense substrates such as fibrous, ballistic resistant body armor [20]. As these challenges are overcome, applications such as high-speed communications, high power, and high frequency data transfer become possible across any surface, reducing the need for separate wiring harnesses and power handling. These potential printed solutions also lack nonintrusive, low-loss connections and suffer from poor long-term reliability and stability. Many successful designs reported within the literature [21] [22] remain relatively bulky and require large commercial off-the-shelf (COTS) coaxial connectors.

Similarly, the adhesion of packaged surface mount devices (SMDs), such as amplifiers or microcontrollers, has also remained a significant challenge for printed RF electronics. For example, wicking of nanoparticle ink into the substrate tends to create unintentional electrical shorting. Additionally, many inks used in printed interconnects require high-temperature and long sintering cycles, which risks critical failure to active electronics [23]. To this end, anisotropic conductive adhesives have received recent interest as a method to prevent electrical shorting, improve interconnect mechanical stability, and reduce the need for multiple high-temperature sintering cycles [24].

Using traditional AM techniques, there have been demonstrations of multilayer circuits [25] as well as conformal antennas [19] [26] and sensors [27]; however, none of these examples have resulted in highly conformal, multilayer devices that also integrate COTS SMDs. As an AM case study, the effect of these concepts on a functional, multilayer, 10 GHz RF detection circuit will be explored. This detection circuit was fabricated within a doubly curved fiberglass laminate nose cone. Ink-filled vias were used to connect individual layers and SMD components such as capacitors and amplifiers. The evaluation of this circuit provides a pathway towards geometrically complex RF structures where structures can remain low-profile while also integrating a complicated additive framework.

This work also provides several solutions to many of these problems, including fully printed, low-loss RF connectors, anisotropic conductive inks, and package attach methods that demonstrate excellent stability over repeated bend cycles. Also explored are fluoropolymer-based coatings that enable substrate planarization and improved printed adhesion [28].

Doubly Curved Multilayer RF Detector

As an initial testbed, a multi-layer, conformal RF detection circuit was designed within an ogive radome (Fig. 1a). This circuit utilizes two bonded layers of Fibrite 7701/7781 E-glass laminate. The first layer, “CS1”, is 1.5 mm thick and contains an AJ5X aerosol-jet patch antenna, which was printed using PV Nanocell silver nanoparticle ink on the convex side of the insert. On the concave side, a ground plane was printed using the same ink and printer. The second Fibrite layer, “CS2”, is 0.76 mm thick and was bonded to the CS1 insert using a 150 µm layer of FM-73 film adhesive. The RF detection circuit, which includes a bandpass filter, signal transmission lines, and power supply lines, was then printed on the concave CS2 surface (Fig. 1b). Discrete COTS SMDs, including capacitor networks, a low noise amplifier (LNA), an envelope detector, and a digital comparator were then connected to the printed traces using Heraeus CL20-11223 nanoparticle ink, sintered at 90°C for 90 minutes. Overall, the circuit can detect an incoming signal through the patch antenna and transmit the signal through two dielectric layers separated

by a ground plane. The circuit then performs amplification, filtering, envelope detection, and analog-to-digital conversion (Fig. 1c).

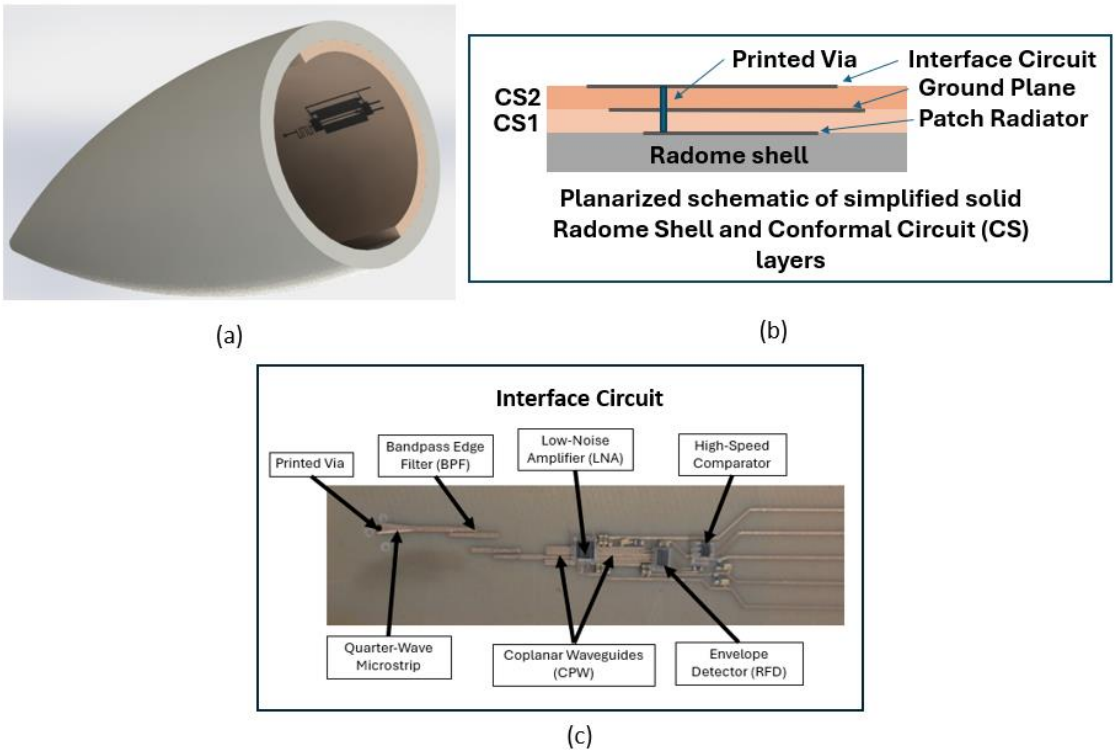

Figure 1. a) Detector circuit shown printed on the CS2 layer that has been fully bonded into the radome. b) The RF detector circuit (interface circuit) was printed on the concave portion of CS2. CS2 was bonded to CS1 which contained a ground plane and patch radiator. The assembly was then bonded onto the inside surface of the radome shell. c) The fully printed interface circuit. A signal is coupled from the patch antenna (CS1) through a printed via to a bandpass filter (CS2). An HMC903 LNA amplifies the signal, which is then converted to an analogue voltage through an ADL6012 envelope detector. An LTC6752 comparator then converts this to a digital output signal.

Mastercam Mill 2019 was used to generate pathing for the Optomec AJ5X. In Mastercam, the CAD of the circuit was imported onto a STEP model of the laminate ogive. Mastercam was then used to compute the raster generation needed to produce uniform line width of 50 µm. To properly align the system, a 1 mm via was used as a fiducial. This via was fabricated using a drill press and connected the patch antenna (CS1) to the detector circuit (CS2), which was filled with Heraeus nanoparticle ink (sintered at 90°C for 90 minutes).

Detector operation was experimentally verified using a Fieldfox N9917A VNA to perform a single port reflected power measurement. This measurement was performed on the RF chain at the interface with the LNA to gauge the resonance frequency of the device. Overall, the circuit demonstrates a maximum power detection at 9.76 GHz with a 124 MHz bandwidth (Fig. 2a), deviating from the 10 GHz design within simulation by 2.46% (Fig 2b).

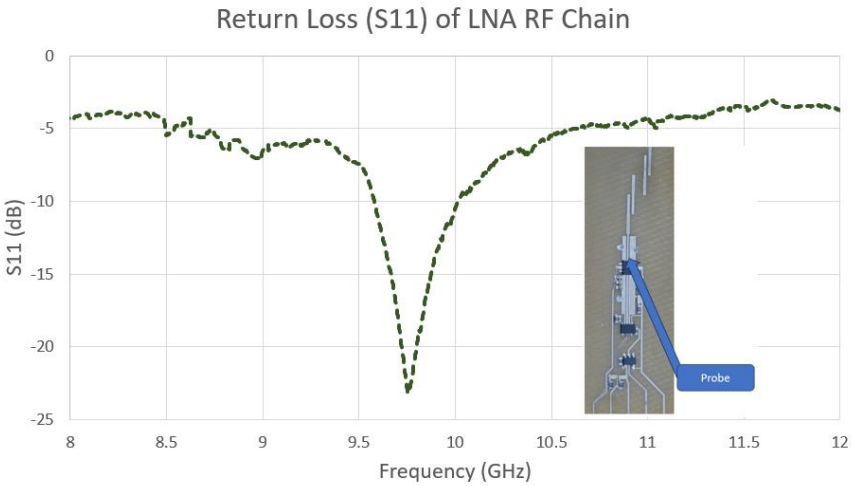

(a)

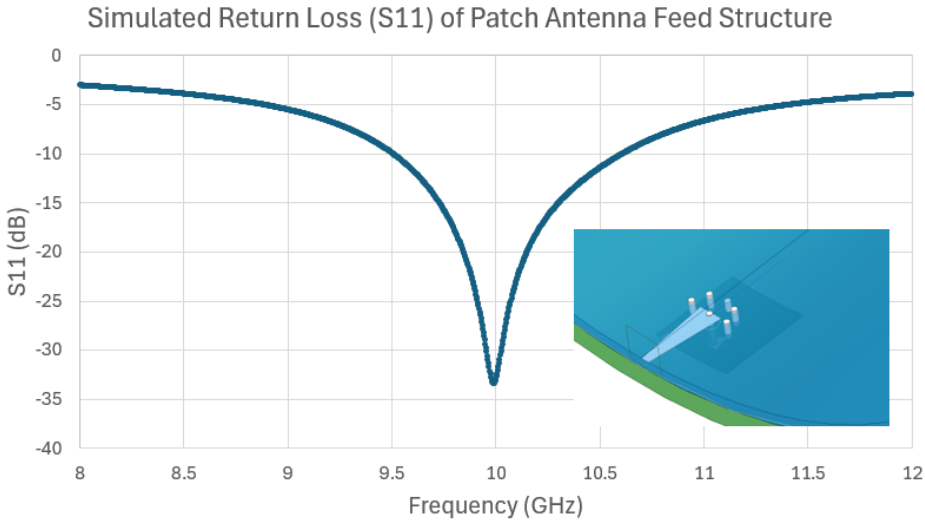

(b)

Figure 2. a) Reflected power of printed RF chain (antenna, bandpass filter, transmission lines) leading into the LNA. b) Reflected power of microstrip-to-patch antenna transmission structure.

Utilizing a standard gain X-band Narda horn, a remote 10 GHz signal was then used to excite the antenna. The resulting signal was measured using the single-ended output voltage and corresponding detected power was obtained by comparing this voltage to the datasheet of the ADL6012 RF detector. The signal was shown to be easily resolvable for various levels of RF input power, and through this analysis, a uniform loss of 18 dB was determined between the printed circuitry, transmission loss, and free-space path loss (Fig. 3). This results in a minimum resolvable transmitter power of -12 dBm (1 mV output).

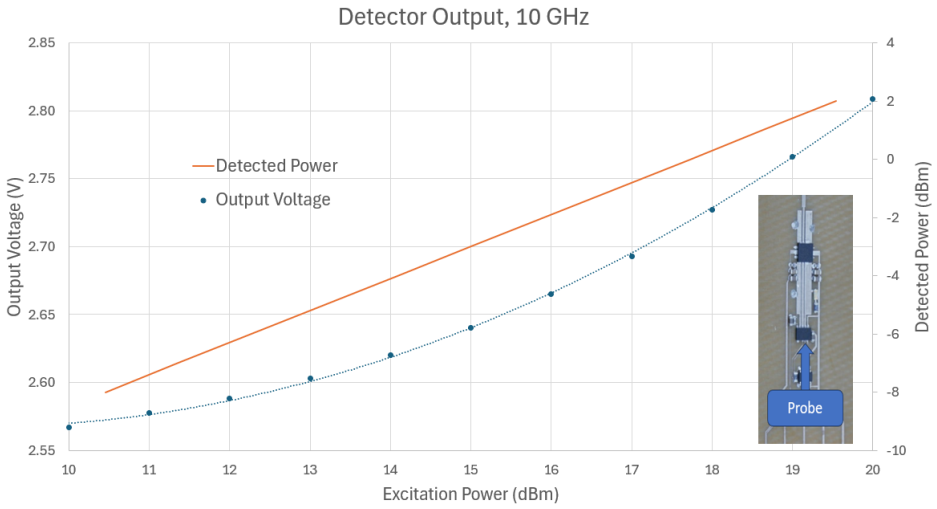

Figure 3. Voltage output of ADL6012 RF detector chip (blue) and corresponding detected power (orange). The realized detector can resolve a minimum transmitter power of -12 dBm.

Despite the functionality of this device (Fig. 4), numerous challenges were faced during the circuit's fabrication. Among these were the roughness of the substrate which resulted in numerous open circuits within the print. Each printed trace showed a measured thickness on the order of 10 µm, and thus small scratches on the substrate resulted in micro-cracks within the ink. These micro-cracks then expanded into high impedance failure points during subsequent heat cycles while placing the RF ICs. Many of the failure points were corrected in the initial printing; however, the resulting circuit performance did not fully recover. Additionally, during testing it was discovered that the electrical connections on the SMD were prone to intermittent failure. Overall, these connections at the SMDs tended to crack when subjected to mechanical stress during handling, bonding, and testing. It is suspected that the initial ink sintering fuses the conductive nano materials and repeated thermal cycling cannot remelt these traces, creating clear interfaces with the addition of more ink [29].

Although there were numerous challenges during fabrication, many of these challenges could be overcome through material, process, and design developments. For example, the inclusion of a fully printable, low loss planarizing coating could reduce the surface roughness of the substrate, and vastly improve both ink reliability and SMD connection reliability. Therefore, this article proposes three methods that can be utilized to improve the reliability and performance of a complex conformal, RF circuit: planarization coatings, anisotropic inks, and electrical/RF connectors.

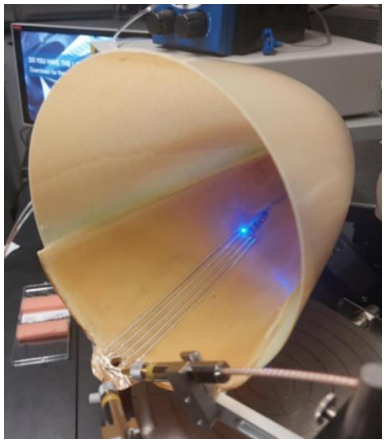

Figure 4. Completed RF detector, powered on and bonded within a radome.

Functionalization of Rough Substrates

To describe a process to planarize and improve adhesion of printed circuits on a non-traditional substrate, this work examines a highly fibrous ultrahigh molecular weight polyethylene laminate (Dyneema HB210). This composite laminate has a thickness of 3.175 mm with each fiber layer rotated 90 degrees and impregnated with a polyurethane resin. Any planarization coatings needed to both functionalize and smooth the laminate before printing and be compatible with Dyneema. Additionally, these coatings were developed to be deposited using three different methods: printing, spray coating, and draw down. During coating development, it was important that the curing temperature of the coating remain less than the melting point of the Dyneema (137℃) and the solvent in the coating should remain unreactive to UHMWPE. As such, 3M Dyneon fluoroplastic THV 221GZ (THV) mixed with triethyl phosphate (TEP) was developed as THV has a melting point of 115℃ and the TEP evaporates from the coating at 130℃ during the curing process.

The two solutions developed for draw down and printing used a solution of 30g THV/100mL TEP and 20g THV/100mL TEP respectively, enabling a more level coating over more precise areas. The 20g THV/100mL TEP solution was viscous enough to self-level during printing, enabling large area coverage using a standard microdispensing printing unit. When spray coating, the solution was designed to be pneumatically atomized with a standard dry air spray nozzle and a solution of 3.33g THV/100mL TEP.

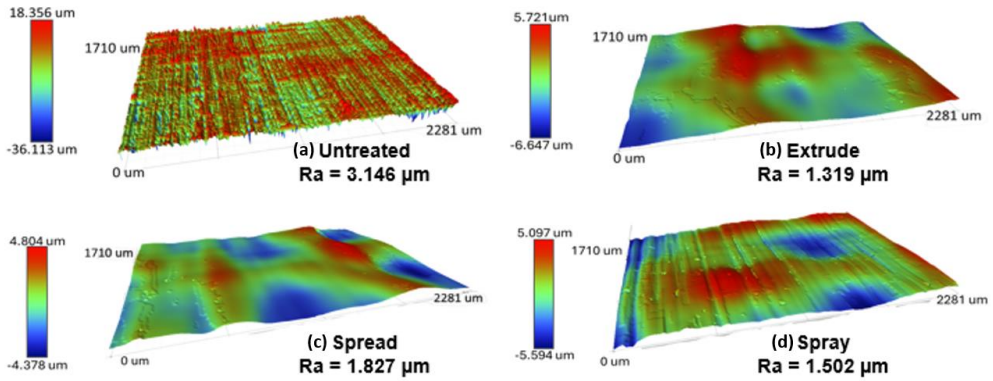

Figure 5. Profilometry scans of (a) uncoated Dyneema substrate, which has a high roughness and a fibrous surface. (b) Dyneema substrate coated with a print process. (c) Dyneema substrate coated with a draw-down process. (d) Dyneema substrate coated with a spray-coat process.

After curing, the surface roughness of the coated and uncoated Dyneema substrate was measured using a Bruker Contour GT Optical Profilometer. Before coating, the average surface roughness (Ra) of the laminate was 3.146 µm (Fig. 5a). After coating the average surface roughness improved to an Ra of 1.827 µm using draw down (Fig. 5c), an Ra of 1.319 µm when printed (Fig. 5b), and an Ra of 1.502 µm when spray coated (Fig. 5d).

DuPont CBO28 silver nanoparticle ink was then printed on the substrates and the adhesion of conductive ink to the coated and uncoated substate was measured using the ASTM D3359 Method B: "Lattice Pattern" standard [30]. When the test was conducted on the non-coated substrate, the adhesion was measured at a classification of 1B with 60% delamination (Fig. 6c, d). The shaded regions of Figure 6 represent ink present before and after testing. When the test was conducted on a coated substrate (Fig. 6a, b), the surface received a classification of 5B with no delamination observed.

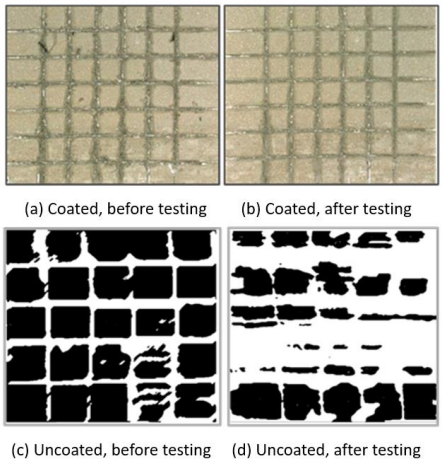

Figure 6. (a) Coated sample before ASTM D3359 pull test. (b) Coated sample after ASTM D3359 pull test, with 0% of sample removed. (c) Uncoated sample before ASTM D3359 pull test. (d) Uncoated sample after ASTM D3359 pull test, with 60% of sample removed.

Evaluation of Anisotropic Ink for Additive Interconnects

To address the challenge of SMD connection reliability to print ink, this work investigated anisotropic conductive epoxies. These epoxies have the unique ability to both improve SMD adhesion and mitigate risk of unintentional contact shorting while also reducing fabrication complexity. As such, Creative Materials 124-19A anisotropic conductive epoxy adhesive was used as a method to secure ICs and surface mount components to printed electrical circuits. This epoxy consists of two parts: "Part A" of the mixture contains the Creative Materials proprietary epoxy resin, silica, and silver conductive spheres. "Part B" of the mixture contains a proprietary blend of the curing agent, dimer diamine and phenol. A mixture of 100A/30B by mass was evaluated for its electrical and mechanical characteristics. This ratio differs from the manufacturer recommendation of 100A/58B which we found increased the concentration of metallic spheres within the epoxy (Fig. 7) and improved circuit reliability.

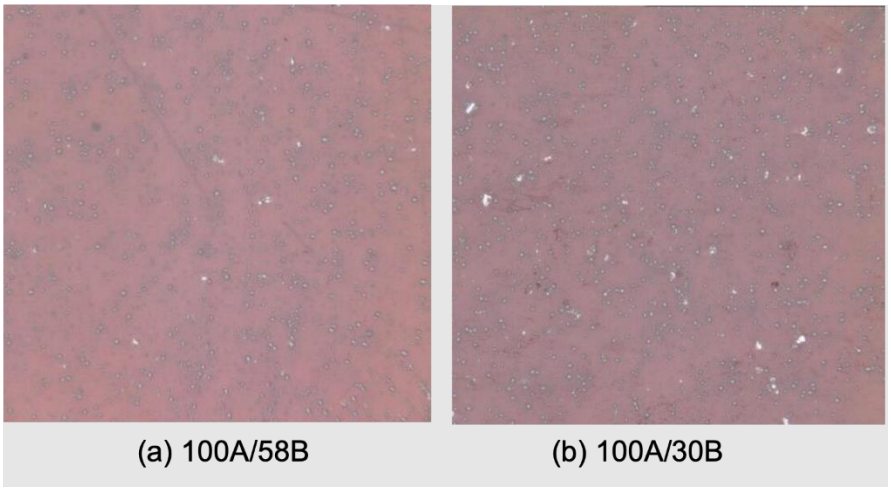

Figure 7. Comparison of the sphere density of (a) the 100mg "Part A" to 58 mg "Part B" mixture recommended by the manufacturer and (b) utilized the 100mg "Part A" to 30 mg "Part B" mixture. The 100A/30B mixture possesses a higher conductive sphere density.

To test the flexural reliability of the anisotropic conductive epoxy, a circuit of five parallel resistors was printed using Heraeus CL20-11223 (sintered at 150°C for 30 min.) and a Nordson Pro4 dispensing system on a 127 µm-thick Kapton polyimide substrate (Fig. 8). After ink sintering, the anisotropic epoxy was printed across the connection pads using the Nordson Pro4 and a 22-gauge needle. Five 0603 SMD 1kΩ resistors were then placed across the contact pads and light pressure was applied over a 24-hour room temperature cure cycle. The resistor network was measured to have an effective resistance of 200Ω, which increases as the resistor connections fail.

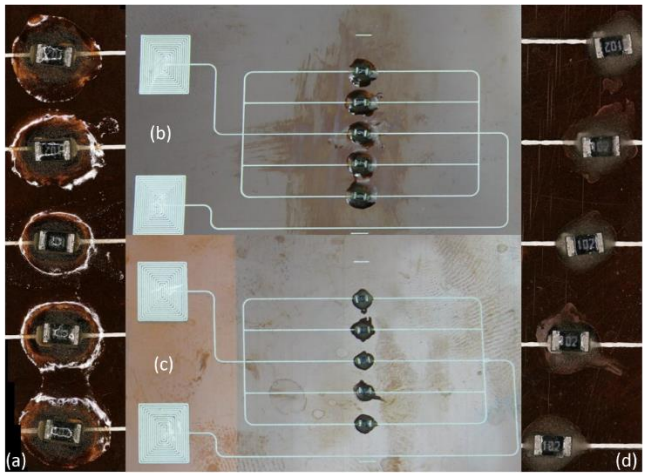

Figure 8. Microscope images of (a) resistor connections fabricated with the 100A/58B mixture, (b) complete resistor network using the 100A/58B mixture, (c) complete resistor network using the 100A/30B mixture, (d) resistor connections fabricated with the 100A/30B mixture.

The circuit was tested over 10,000 bends with resistance measurements recorded after every 10 bends. No failures were observed until approximately 8,000 bends for the 100A/30B mixture (Fig. 9). Additionally, a resistance drift of approximately 10 Ω was observed throughout the bend testing due to movement of the conductive spheres within the epoxy matrix. The resistor circuit was also temperature cycled 125 times within an ESPEC BTL-433 environmental chamber from 0°C to 120°C at a rate of 1.5 °C/min. The circuit's total resistance after cycling was consistent with the measurement taken before the temperature cycling occurred (Table 1), implying some environmental stability over this temperature range.

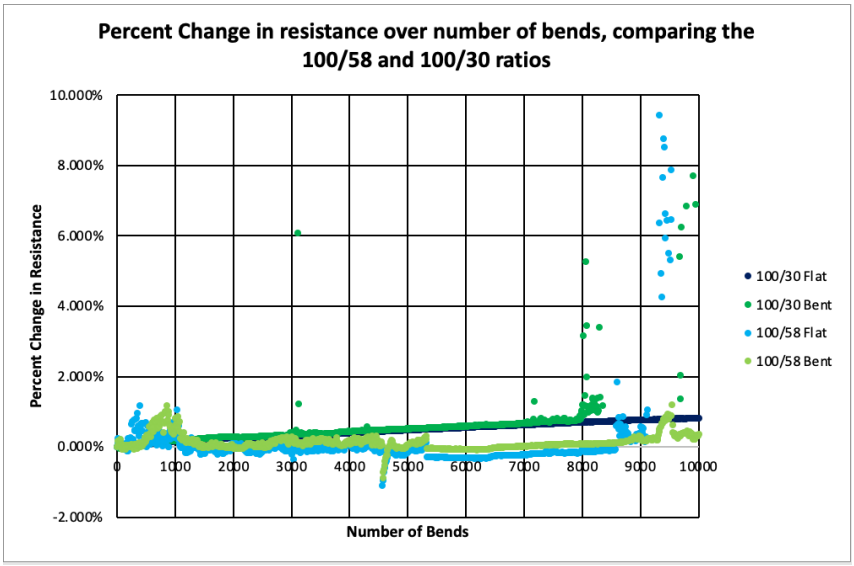

Figure 9. Change in resistance over 10,000 bending cycles. The 100A/30B sample experiences a 1% drift over 10,000 cycles when flattened (black), with a spike in resistance seen during bending at 8,000 cycles (dark green). The recommended 100A/58B sample does not see as significant of a drift (blue) but has more connection failures during bending (light green).

	Before Temp Cycle	After Temp Cycle
Measured Resistance (Ω)	214.32 Ω	215.16 Ω

Table 1. Experimental resistance before and after temperature cycling. There is a lack of appreciable change after 125 cycles implying some environmental stability of the connection method.

A second circuit was designed to evaluate anisotropic inks as a method to incorporate QFN and DFN packages into printed electronic circuits The circuit in question consisted of two 0603 1kΩ resistors, two 0603 blue LEDs, and a PIC16 microcontroller on a glass substrate (Fig. 10). The circuit was once again printed with Heraeus CL20-11223 (sintered at 150°C for 30 minutes). The anisotropic epoxy was printed immediately after this, the components were placed, and the resulting circuit was then cured at room temperature for 24 hours. This device is shown in Figure 10 and demonstrated full functionality through all discrete components and microcontroller pins.

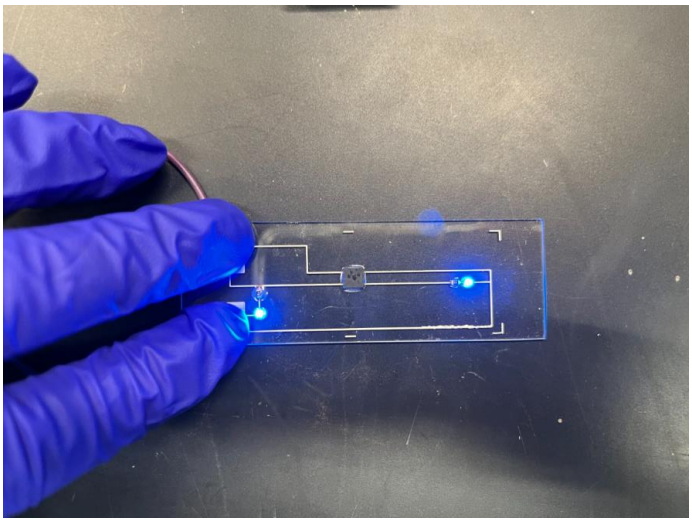

Figure 10. Functional microcontroller circuit atop glass substrate using anisotropic conductive epoxy for component interconnections.

This epoxy for component interconnections shows strong promise for conformal electronic systems. For example, this ink could replace the current connections within the multilayer RF detector nose cone of section 2. The result would be reduced failure at the critical SMD/ink interface. This improvement would be even more evident as the requirement for environmental stability becomes more prevalent.

Printed Microwave Connectors

The final major failure point of the demonstration unit in section 2 was the electrical connections between the nose cone circuit and external circuitry. An additively manufactured RF connector may overcome some of these challenges as it could be moved towards custom RF functionality and specialized locking mechanism for attaching, aligning, and grounding multiple coplanar waveguides (GCPWs) and DC connections. GCPWs are a commonly used RF transmission line structure due to high signal isolation and transmission efficiency [31]. The printed connector in this work was fabricated using printed polyether ether ketone (PEEK) as a

dielectric, due to its low loss and high temperature stability. PEEK has an average dielectric constant (ε_r) of 3.01 and a loss tangent ($tan(\delta)$) of 0.0028 over the passband of 1-6 GHz [32], which was characterized using a Keysight N5222A PNA using the Nicholson-Ross-Weir method [33]. Conductive traces were printed using Dupont CB028 silver nanoparticle ink and all simulations were performed using Ansys HFSS.

The printed PEEK connector was designed with a characteristic impedance of 50Ω for compatibility with most monolithic microwave integrated circuits (MMICs). A series of 0.6mm diameter vias with a uniform 0.95mm spacing were inserted into the design to improve isolation and prevent unintentional mode excitations between the surface and bottom ground planes (Fig. 11b). Parametric analyses were performed using Ansys HFSS to obtain optimal feature sizing.

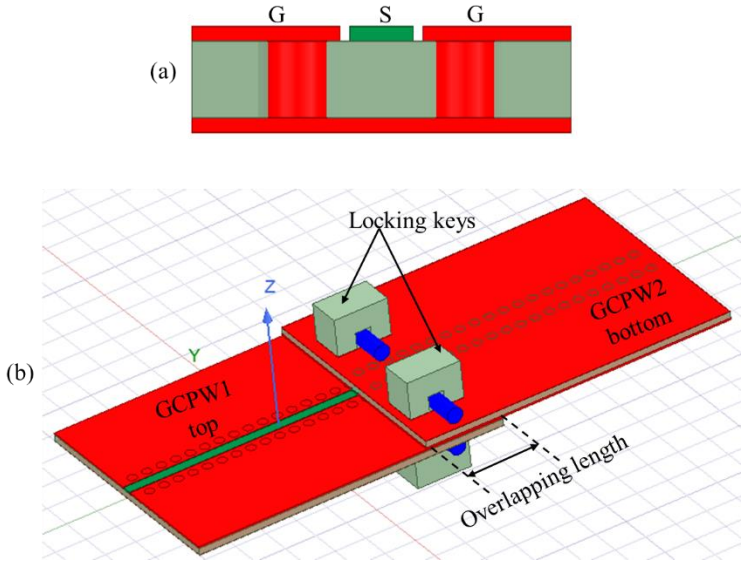

Figure 11. (a) Cross-section of the GCPW ground-signal-ground. (b) Isometric view of the printed connector. A set of two locking keys are used to apply pressure to the two mating GCPWs to maintain an electrical connection.

The PEEK substrate was extruded using fused deposition modelling (FDM) on a Hyrel Hydra 3D printer and metalized using Dupont CBO28 (cured for 6 hours at 95°C) in a drawdown process. The Hyrel's CNC tool head was used to pattern the ground-signal-ground features of the GCPW. To fabricate isolation vias between the two ground planes, an LPKF Protomat was used and the vias (20 vias on each GCPW) were metalized with conductive ink,

The transmission performance of the connector was characterized with a Fieldfox N9917A and compared to simulation. The printed device demonstrated low transmission loss (S21) over the passband of 1 – 6 GHz and reflected power (S11) only exceeding -10 dB at 6 GHz. As such, this printed connector shows significant promise for low-profile interconnection between multiple printed devices, greatly increasing the utility of custom RF circuits and systems.

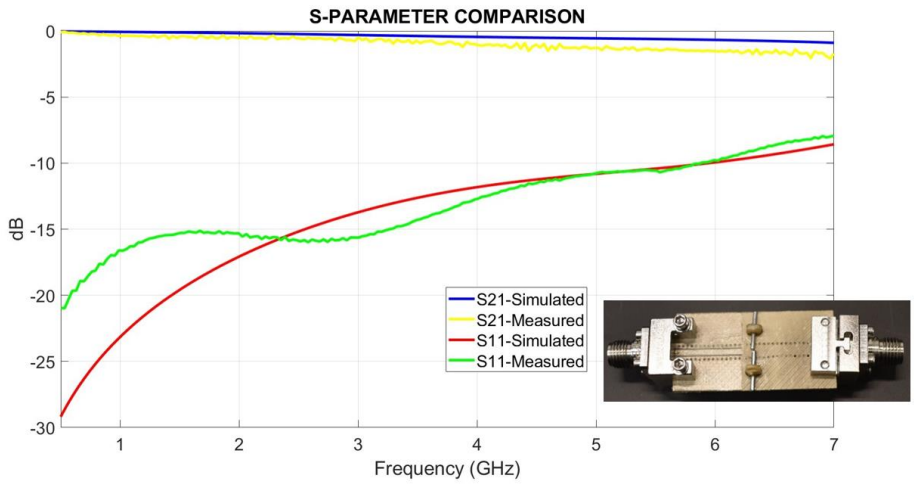

Figure 12. Comparison between simulated and experimental data for power transmitted (S21) and power reflected (S11) by the printed connector.

Summary and Future Work

Additive manufacturing has greatly expanded the versatility of RF electronics, enabling applications with nontraditional form factors embedded directly into existing structures. Despite this, much of the work within the literature has been focused on fabricating advanced electronics, with little insight into directly addressing the challenges of reliable, highly conformal, multilayer systems. This work demonstrates the challenges in fabricating such a device, i.e. a doubly curved, multilayer RF detector integrated directly within an ogive nosecone. The detector was able to demonstrate full functionality a resonance frequency of 9.76 GHz with minimum resolvable transmission power of -12 dBm. Despite this success, numerous challenges were faced in the circuit's fabrication, including surface roughness induced faults, poor adhesion, and unreliable electrical connections. As such, this work also explores several solutions to these problems. A low-loss, fluoropolymer coating dissolved in TEP was developed which can be applied using spray coating, printing, and draw down. This coating increased adhesion to near 100% and reduced surface roughness by at least a factor of two. An anisotropic epoxy was also described that improves both adhesion and connection reliability over 8,000+ bend cycles and 125 temperature cycles from 0°C to 120°C. Additionally, this anisotropic material system utilized a room-temperature cure process that could be applicable to a wide range of ICs without damaging the components. Finally, a fully printed, low-loss RF connector was developed that enables a wide array of devices to seamless connect over a GCPW interface. This connector was fully printed in a single AM tool and demonstrated less than 2 dB of return loss from 0-6 GHz.

This work demonstrates the need for multiple solutions and multiple interwoven research areas for the saucerful adoption of AM RF by broader industry. The solutions presented in this work have the potential to enable high-yield fabrication of complex conformal RF structures using purely additive techniques if the correct materials, processes, and designs are followed. AM allows designers to formulate unique and dynamic solutions to existing challenges faced within RF design, but the field must be willing to adopt even more novel techniques to demonstrate applicability to the challenges of today's commercial market.

Acknowledgements

This research was funded by HEROES ASPIRE II initiative and the DEVCOM Soldier Center under BAA W911QY-20-2-0005 and BAA W911QY-18-2-0006, NextFlex 7.2 under General Dynamics Mission Systems subcontract 22-SC-0053, and UML's Francis College of Engineering. This material is based upon work supported by the National Science Foundation under Grant No. 2120581.

The authors would like to acknowledge the support of the Kansas City National Security Campus (KCNSC). Honeywell Federal Manufacturing & Technologies, LLC operates the Kansas City National Security Campus for the United States Department of Energy/National Nuclear Security Administration under Contract Number DE-NA0002839.

References

[1] R. A. Mellita, S. S. Karthikeyan and P. Damodharan, "Additively Manufactured Conformal All-dielectric Frequency Selective Surface," *2020 50th European Microwave Conference (EuMC)*, pp. 772-775, 2021.

[2] X. Konstantinou, M. T. Craton, J. D. Albrecht and J. Papapolymerou, "Ultra-Wideband Transmission Lines on Complex Structures via Extendable Aerosol Jet 3D-Printing," *2021 IEEE International Conference on Microwaves, Antennas, Communications and Electronic Systems (COMCAS)*, pp. 103-106, 2021.

[3] D. Helena, A. Ramos, T. Varum and J. N. Matos, "Antenna Design Using Modern Additive Manufacturing Technology: A Review," *IEEE Access*, vol. 8, pp. 177064-177083, 2020.

[4] G. S. Khinda, A. Umar, R. Cadwell and M. Alhendi, "Flexible inkjet-printed Patch antenna array on mesoporous PET substrate for 5G applications with stable RF performance after mechanical stress cycling," in *2020 IEEE 70th Electronic Components and Technology Conference (ECTC)*, Lake Buena Vista, FL, 2020.

[5] H. F. Abutarboush and A. Shamim, "A Reconfigurable Inkjet-Printed Antenna on Paper Substrate for Wireless Applications," *IEEE Antennas and Wireless Propagation Letters*, vol. 17, no. 9, pp. 1648-1651, 2018.

[6] C. M. Shemelya, M. Zemba, M. Liang, D. Espalin, C. Kief, H. Xin, R. B. Wicker and E. W. MacDonald, "3D printing multi-functionality: Embedded RF antennas and components," in *2015 9th European Conference on Antennas and Propagation (EuCAP)*, Libson, Portugal, 2015.

[7] Z. Chai, S. A. Abbasi and A. A. Busnaina, "Additively Manufactured Zinc Oxide Thin-Film Transistors Using Directed Assembly," *ACS Applied Electronic Materials*, vol. 5, no. 4, pp. 2328-2337, 2023.

[8] M. M. Abdin, W. J. D. Johnson, J. Wang and T. M. Weller, "W-Band MMIC Chip Assembly Using Laser-Enhanced Direct Print Additive Manufacturing," *IEEE*

Transactions on Microwave Theory and Techniques, vol. 69, no. 12, pp. 5381-5392, December 2021.

[9] A. Guennou-Martin, Y. Quere, E. Rius, L. Fourtinon, C. Person, G. Lesueur and T. Merlet, "Design and manufacturing of a 3-D conformal slotted waveguide antenna array in Ku-band based on Direct Metal Laser Sintering," in *2016 IEEE Conference on Antenna Measurements & Applications (CAMA)*, Syracuse, NY, USA, 2016.

[10] C. Stoumpos, T. L. Gouguec, R. Allanic and M. García-Vigueras, "Compact Additively Manufactured Conformal Slotted Waveguide Antenna Array," *IEEE Antennas and Wireless Propagation Letters,* vol. 22, no. 8, pp. 1843-1847, August 2023.

[11] E. Gupta, C. Bonner, N. Lazarus, M. S. Mirotznik and K. J. Nicholson, "Multiaxis Manufacture of Conformal Metasurface Antennas," *IEEE Antennas and Wireless Propagation Letters,* vol. 22, no. 11, pp. 2629-2633, November 2023.

[12] G.-L. Huang, S.-G. Zhou, T.-H. Chio and T.-S. Yeo, "Fabrication of a High-Efficiency Waveguide Antenna Array via Direct Metal Laser Sintering," *IEEE Antennas and Wireless Propagation Letters,* vol. 15, pp. 622-625, 2016.

[13] M. Liang, W.-R. Ng, K. Chang, K. Gbele, M. E. Gehm and H. Xin, "A 3-D Luneburg Lens Antenna Fabricated by Polymer Jetting Rapid Prototyping," *IEEE Transactions on Antennas and Propagation,* vol. 62, no. 4, pp. 1799-1807, April 2014.

[14] K. Adria, S. Khushrushahi, G. Strack and A. Alkim, "Printed Metasurfaces for Wearables," in *2022 IEEE International Symposium on Antennas and Propagation and USNC-URSI Radio Science Meeting (AP-S/URSI)*, Denver, CO, USA, 2022.

[15] A. M. Nicolson and G. F. Ross, "Measurement of the Intrinsic Properties of Materials by Time-Domain Techniques," *IEEE Transactions on Instrumentation and Measurement,* vol. 19, no. 4, pp. 377-382, November 1970.

[16] K. Berry, E. M. Brown, B. Pothier, S. Fedorka, A. Akyurtlu, C. Armiento, G. F. Walsh and C. M. Shemelya, "Overcoming Variability in Printed RF: A Statistical Method to Designing for Unpredictable Dimensionality," *Designs,* vol. 6, no. 1, p. 13, 2022.

[17] B. L. Gray, "The Textile is the Substrate: Challenges of Direct-on-Fabric Wearables," in *Conference: 2023 IEEE International Flexible Electronics Technology Conference (IFETC)*, San Jose, CA, USA, 2023.

[18] A. P. Golhin, "Surface roughness of as-printed polymers: a comprehensive review," *The International Journal of Advanced Manufacturing Technology,* vol. 127, p. 987–1043, 2023.

[19] Y. H. Wang, D. X. Du, H. Xie, X. B. Zhang, K. W. Lin and E. Fu, "Printability and electrical conductivity of silver nanoparticle-based conductive inks for inkjet printing," *Journal of Materials Science: Materials in Electronics,* vol. 32, p. 496–508, 2021.

[20] B. J. Pothier, *Additively Manufactured 5G Antenna Structures on Functional Polyethylene Substrates*, Lowell, MA, USA: University of Massachusetts Lowell, 2022.

[21] J. Kuhling, R. Dahle, D. Chowdhry and P. Laforge, "Applying additive manufacturing to integrate coaxial connectors with 3D printed waveguides for cascaded RF link applications," *Additive Manufacturing*, vol. 35, October 2020.

[22] K. Mcparland, Z. Larimore, P. Parsons, A. Good, J. Suarez and M. Mirotznik, "Additive Manufacture of Custom Radiofrequency Connectors," *IEEE Transactions on Components, Packaging and Manufacturing Technology*, vol. 12, no. 1, pp. 168-173, January 2022.

[23] Y. Zhong, R. An, H. Ma and C. Wang, "Low-temperature-solderable intermetallic nanoparticles for 3D printable flexible electronics," *Acta Materialia*, vol. 162, pp. 163-175, 2019.

[24] R. N. Das, J. M. Lauffer and F. D. Egitto, "Electrical conductivity and reliability of nano- and micro-filled conducting adhesives for z-axis interconnections," in *56th Electronic Components and Technology Conference*, San Diego, CA, USA, 2006.

[25] M. Li, Y. Yang, F. Iacopi, M. Yamada and J. Nulman, "Compact Multilayer Bandpass Filter Using Low-Temperature Additively Manufacturing Solution," *IEEE Transactions on Electron Devices*, vol. 68, no. 7, pp. 3163-3169, July 2021.

[26] L. Josefsson and P. Persson, Conformal array antenna theory and design, Piscataway, NJ: IEEE Press, 2010.

[27] W. Gao, . S. Emaminejad, . H. Y. Y. Nyein, S. Challa, K. Chen, A. Peck, H. M. Fahad, H. Ota, H. Shiraki, D. Kiriya, D.-H. Lien, G. A. Brooks, R. W. Davis and A. Javey, "Fully integrated wearable sensor arrays for multiplexed in situ perspiration analysis," *Nature*, vol. 529, no. 7587, pp. 509-514, January 2016.

[28] R. M. Stephenson and S. Malanowski, Handbook of the Thermodynamics of Organic Compounds, 1st ed., Springer, 1987.

[29] A. Hussain, H. . L. Lee and S. J. Moon, "Sintering of silver nanoparticle structures and the pursuit of minimum resistivity," *Materials Today Communications*, vol. 34, 2022.

[30] ASTM International, "Standard Test Methods for Rating Adhesion by Tape Test," 7 March 2023. [Online]. Available: https://www.astm.org/d3359-23.html. [Accessed June 2024].

[31] J. Kasule, A. Akyurtlu and C. Armiento, "High Speed Digital Signaling in Printed, Planar Microwave Connectors with Multiple Signal Lines," in *2023 IEEE 32nd Conference on Electrical Performance of Electronic Packaging and Systems (EPEPS)*, Milpitas, CA, 2023.

[32] J. Kasule, A. Akyurtlu and C. Armiento, "Printed, Planar Microwave Connector with Multiple Signal Lines," in *IEEE Annual Conference on Wireless and Microwave Technology (WAMICON)*, Melbourne, FL, 2023.

[33] A. M. Nicolson and G. F. Ross, "Measurement of the Intrinsic Properties of Materials by Time-Domain Techniques," *IEEE Transactions on Instrumentation and Measurement,* vol. 19, no. 4, pp. 377-382, November 1970.